Synthesis, Spectroscopic Characterization and DFT Calculations of a Novel Lanthanum Complex of Ferrocenyl Dithiophosphonate

A. Aydin* AND B. Dede

Süleyman Demirel University, Faculty of Sciences & Arts, Department of Chemistry, 32260, Isparta, Türkiye

In this study, a novel lanthanum complex based on ferrocenyl (Fc) dithiophosphonate was synthesized and characterized, and quantum chemical calculations were performed. The reaction of 2,4-diferrocenyl-1,3-dithiadiphosphetane disulfide dimer $[FcP(\mu\text{-}S)S]_2$ (ferrocenyl Lawesson reagent: FcLR) with iso-propyl alcohol (^iPr) gave the O-alkyl ester ($[FcPS(OR)SH]$, R= ^iPr), and the ester was converted to its ammonium salt, $[NH_4L]$ **(1)**, where L was the ferrocenyl phosphonodithioate anion. A novel lanthanum complex was prepared by the reaction of $[NH_4L]$ with the salt of $La(NO_3)_3 \cdot 6H_2O$ in tetrahydrofuran solvent, thus giving $[[LaL_2]NO_3 \cdot 4H_2O]$ **(2)**. The synthesized compounds were characterized using (^1H, ^{31}P) nuclear magnetic resonance, Fourier transform infrared, thermal, and elemental analysis. Density functional calculations of both compounds were performed in order to obtain valuable information about the electronic structures, properties, and reactivity of the synthesized molecules. Optimized geometries, molecular electrostatic potential surface, and HOMO–LUMO orbitals of the compounds **1** and **2** were calculated with a 6-311G(d, p) basis set using density functional theory and B3LYP functional. LanL2DZ with an effective core potential for the Fe and La atoms was used.

topics: dithiophosphonate, ferrocenyl phosphonic acids, lanthanum complex, density functional theory (DFT)

1. Introduction

Regarding organophosphorus derivatives, there is numerous literature available on the synthesis and characterization of dithiophosphate $[S_2P(OR)_2]^-$ and dithiophosphinate $[S_2PR_2]^-$ and its complexes. However, due to synthetic difficulties, dithiophosphonate $[S_2PR(OR)]^-$ compounds and lanthanide complexes have not been reported to be studied extensively [1–3]. Dithiophosphonic acid and its derivatives are used as an additive for preventing oxidation and abrasion in hydraulic systems, lubricating oils, as well as plasticizing additives in the production of polymeric materials, as they are easily soluble in oils [4–6]. Lanthanum-based complexes have been extensively studied for their diverse applications in catalysis and materials science due to their unique properties, such as redox activity and magnetic behavior [7, 8]. Lanthanum complexes have also been investigated for their applications in biomedicine and optical applications [9, 10]. Among various lanthanum complexes, ferrocenyl dithiophosphonate-based complexes have attracted considerable interest due to their unique redox and magnetic properties [11].

Synthesis of lanthanide and actinide complexes can be challenging due to several factors. First, the lanthanides and actinides have relatively similar chemical properties, making it difficult to selectively form complexes with a particular element. This can be especially challenging when attempting to form complexes with specific oxidation states, which can vary depending on the ligands used and the reaction conditions. In addition, the lanthanide and actinide ions have large ionic radii and tend to form coordination complexes with high coordination numbers, often with covalent and ionic bonding components, which can result in complex and intricate structures. This complexity can make the synthesis and characterization of these complexes difficult. Due to these difficulties, the lanthanum complexes we synthesized in this study are relatively few in the literature.

On the other hand, density functional theory (DFT) is a computational tool that has revolutionized the field of chemistry by allowing for accurate predictions of molecular structures, reactivity, and spectroscopic properties. DFT calculations have become an essential tool in the study of chemical systems, particularly in the investigation of complex
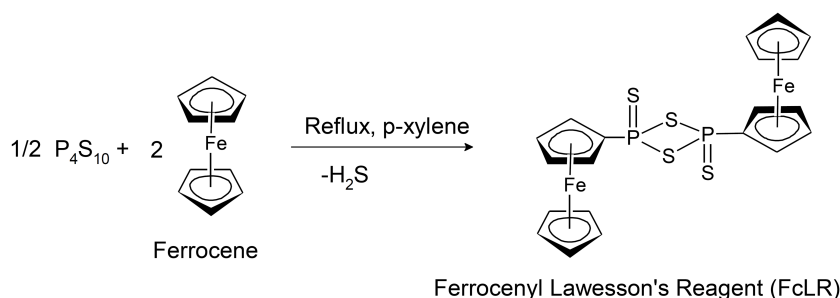
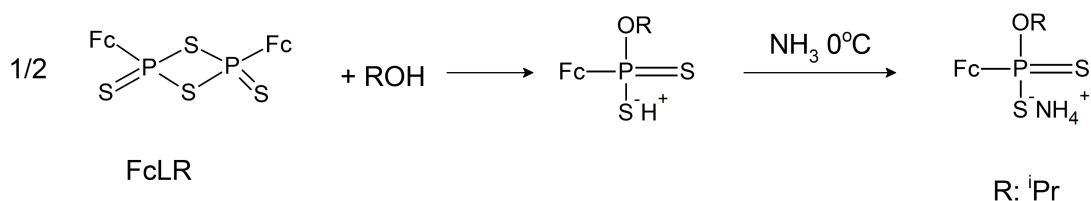Fig. 1.   Synthesis of the ferrocenyl Lawesson's reagent (FcLR).

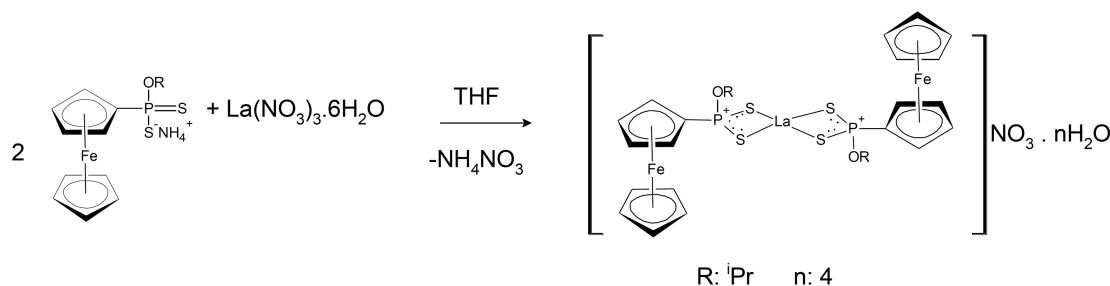Fig. 2.   Synthesis of the ammonium ferrocenyl dithiophosphonate (**1**).

Fig. 3.   Synthesis of lanthanum complex based on ferrocenyl dithiophosphonate (**2**).

molecules and materials. DFT calculations can provide valuable insights into the electronic structure and properties of a molecule or material, such as electronic density distribution, bond lengths, bond angles, and vibrational frequencies.

Within the scope of this study, first, 2,4-diferrocenyl-1,3-dithiadiphosphetane disulfide dimer with the general formula $[FeC_{10}H_9P(S)S]_2$ (ferrocenyl Lawesson's reagent) was synthesized from the stoichiometric reaction of phosphorus pentasulfide dimer (P_4S_{10}) and ferrocene $[Fe(C_5H_5)_2]$ in the presence of solvent (Fig. 1).

As a result of the addition of iso-propyl alcohol (^iPr) to the dimeric structure of ferrocenyl Lawesson's reagent, ferrocenyl dithiophosphonic acid O-alkyl ester was synthesized and treated with anhydrous ammonia gas and isolated from the medium as the ammonium salt [12, 13] (Fig. 2).

La(III) complex was synthesized from the reaction of the prepared ferrocenyl dithiophosphonic acid O-alkyl ester ammonium salt with $La(NO_3)_3 \cdot 6H_2O$ salt in the tetrahydrofuran (THF) medium [14].

With the assumption of four coordination, the reaction equation can be written as shown in Fig. 3.

The structures of the synthesized compounds were researched using elemental analysis, thermal analysis, and Fourier transform infrared (FT-IR) and, (^1H, ^{31}P) nuclear magnetic resonance (NMR) spectroscopy.

2. Material and methods

2.1. Physical measurements

Melting points were determined with a Gallenkamp apparatus without correction. Elemental analyzes were done using the LECO CHNS-932 instrument. Infrared (IR) spectra were recorded with a Mattson-1000 FTIR spectrometer using KBr pellets in the 4000–400 cm^{-1} range. ^1H- and ^{31}P-NMR spectra were recorded in DMSO-d_6 on Bruker DPX 400 FT-NMR spectrometer. Thermal analyses were carried out by using Perkin Elmer Diamond TGA thermal analyzer.
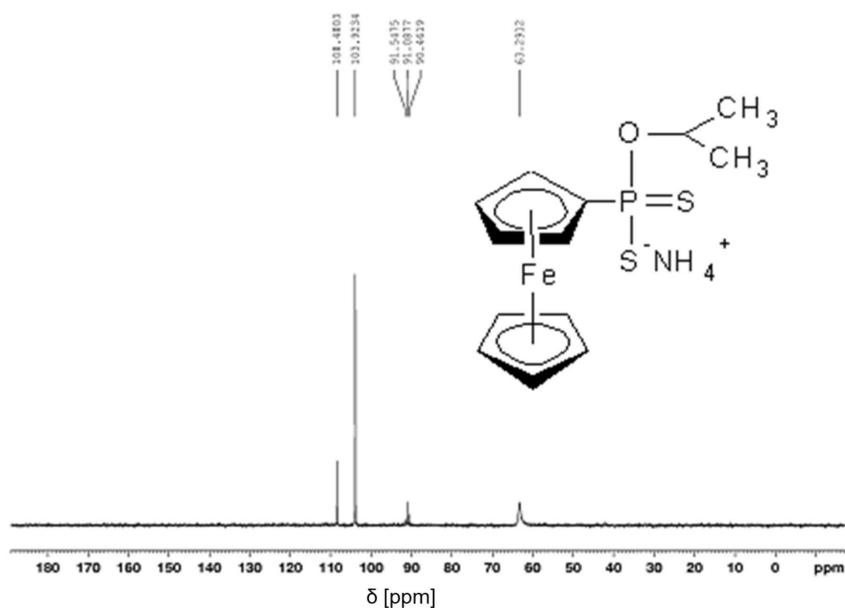
Fig. 4. ^{31}P-NMR spectrum of compound **1** recorded in DMSO-d$_6$.

2.2. Synthesis of ammonium O-iso-propyl ferrocenyl dithiophosphonate (NH$_4$L) **(1)**

NH$_4$L was prepared in accordance with the literature published for related compounds [14]. Dry iso-propyl alcohol (0.6 mL, 8 mmol) was dissolved in dry toluene (80 mL), and the solution was added to the ferrocenyl Lawesson's reagent (FcLR) (2 g, 4 mmol) at 70–80°C. The mixture was then heated until complete dissolution of solids was observed. The reaction vessel was allowed to cool down to room temperature. Then the vessel was placed in an ice bath, and anhydrous NH$_3$ slowly bubbled through, resulting in the formation of a bright yellow precipitate. The precipitated solid was filtered, washed with toluene and diethylether, and dried in a vacuum desiccator.

In summary:

- yield: 2.1 g (82%);
- melting point: 176°C;
- elemental analysis: anal. calc. for [Fc(OC$_3$H$_7$)PS$_2$]$^-$NH$_4^+$: C, 43.95; H, 5.11; S, 18.05 ; N, 3.94% found: C, 44.34; H, 5.45; S, 15.42; N, 2.96%.

2.3. Synthesis of [bis-O-iso-propyl ferrocenyl dithiophosphonate] lanthanum(III) nitrate tetrahydrate complex **(2)**

To the solution of 0.25 g of ammonium O-iso-propyl ferrocenyl dithiophosphonate compound in 10 mL THF in a 100 mL flask fitted with a refluxer, 0.1 g La(NO$_3$)$_3 \cdot$ 6H$_2$O dissolved in 10 mL THF at stoichiometric ratio was added dropwise. The mixture was heated for 5–10 min. Solid NH$_4$NO$_3$

formed as a result of the reaction was removed by filtration. The oily substance obtained was solidified with diethyl ether. The obtained solid was washed with alcohol and left to crystallize in a dichloromethane-methanol (1:1) mixture. The complex was obtained as a dark green precipitate. It was washed with diethyl ether and dried in a vacuum desiccator.

In summary:

- yield: 0.16 g (75%);
- decomposition point: 168°C;
- elemental analysis: anal. calc. for LaP$_2$S$_4$Fe$_2$C$_{26}$H$_{40}$NO$_9$: C, 32.82; H, 4.24; S, 13.48% found: C, 30.59; H, 3.02; S, 13.70%;
- IR (KBr): 3400 cm^{-1} (ν_{O-H}), 1389 cm^{-1} (ν_{N-O}), 1182 cm^{-1} (ν_{P-O-C}), 672 cm^{-1} ($\nu_{asym(PS)}$), 563 cm^{-1} ($\nu_{sym(PS)}$).

2.4. Computational details

All calculations and visualizations were performed using Gaussian 09 and GaussView 5.0.9 program packages, respectively [15, 16]. Optimized geometries, vibrational wavenumbers, molecular electrostatic potential (MEP) surfaces, HOMO and LUMO of the **1** and **2** (closed-shell) molecules were calculated by the DFT method at the B3LYP level using the 6-311G(d, p) basis set for C, H, O, P, and S [17, 18]. LanL2DZ with an effective core potential for the Fe and La atoms was used [19]. The calculated vibrational wavenumbers were scaled with a factor of 0.9682 for frequencies greater than 1700 cm^{-1} and of 1.0119 for frequencies less than 1700 cm^{-1} in order to avoid systematic errors [20].

TABLE I

^{1}H-NMR chemical shifts (δ) of the synthesized compounds (in ppm).

Compound	P–OCH-	-(CH$_3$)$_2$	-Fc$_{(subs)}$	-Fc$_{(subs)}$	-Fc$_{(unsubs)}$	^{31}P
[Fc(OC$_3$H$_7$)PS$_2$]$^-$NH$_4^+$ (**1**)	4.40 (m,H)	1.00 (d,6H)	4.42 (b,2H)	4.17 (m,2H)	4.17 (b,5H)	103
LaP$_2$S$_4$Fe$_2$C$_{26}$H$_{40}$NO$_9$ (**2**)	4.41 (broad)	1.20 (d,12H)	4.42 (broad)	4.17 (broad)	4.21 (broad)	20–75

s — singlet, d — doublet, dd — doublets of doublets, m — multiplet, b — broad
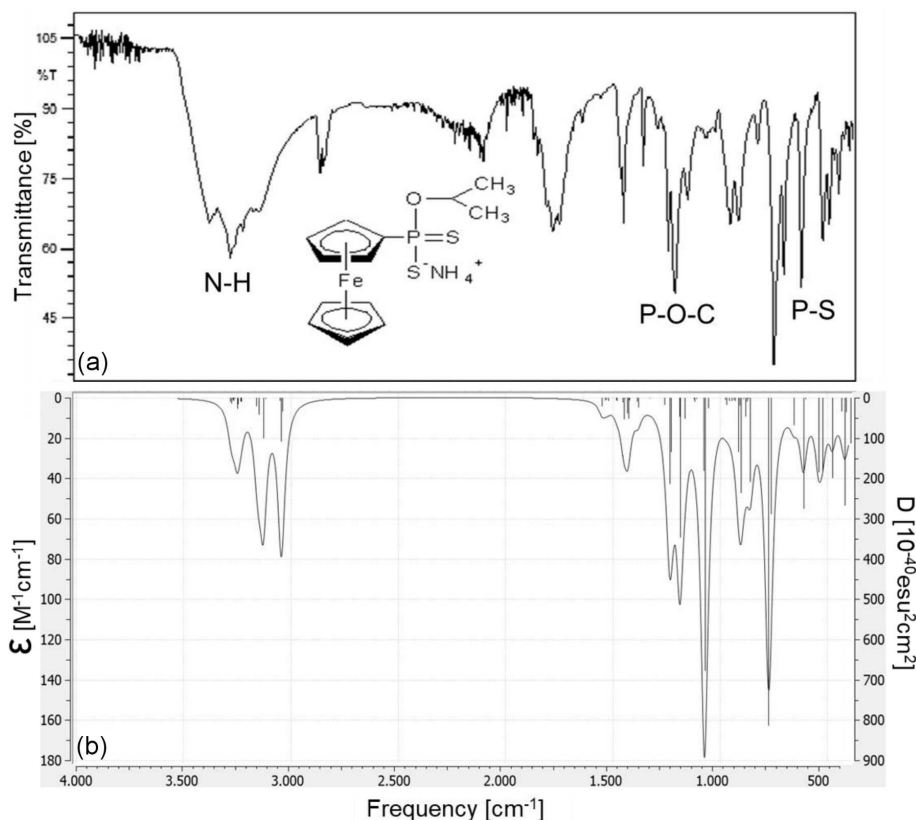
Fig. 5. Experimental (a) and calculated (b) FT-IR spectra of **1**.

3. Results and discussion

3.1. Spectroscopic and thermal properties

It was observed that the ferrocenyl dithiophosphonate salt was stable in a solution and in a solid state. Although different solvents were tried, single crystals of the complex **2** suitable for X-ray could not be obtained. The ^{31}P-NMR spectrum was recorded in DMSO-d$_6$, and the chemical shift value observed at $\delta = 103$ ppm indicated that the compound contains one type of phosphorus (Fig. 4).

It was seen from the ^{1}H-NMR spectrum of the compound that both the ferrocene and alkoxy groups were within the expected chemical shift ranges (Table I). The peaks at $\delta = 4.42$ ppm (b,2H) and 4.17 pmm (b,2H), observed in the phosphorus-interacting ^{1}H-NMR spectrum of compound **1** recorded in DMSO-d$_6$ medium, belonged to protons in the phosphorus-bound ferrocene ring.

It was observed that the peak at $\delta = 4.17$ ppm remained below the unsubstituted ferrocene ring peak. While these peaks should have been observed as a doublet (doublet of doublets) by being cleaved by the neighboring proton and phosphorus, it turned out that these splits were not observed at all. The broad peak at $\delta = 4.17$ pmm (b,5H) was indicated as belonging to the protons in the unsubstituted ferrocene ring. The peak abundance at $\delta = 4.40$ ppm belongs to the -CH- protons in the alkyl group and has been cleaved into two by the phosphorus and into seven by the two adjacent methyl protons and in fact, it should be observed as a 14-point peak. However, a peak abundance was seen in the spectrum. The double peak at $\delta = 1.00$ ppm belongs to two methyl protons and was cleaved by the -CH proton.

Experimental and theoretical IR spectra of the synthesized ferrocenyl dithiophosphonate salt (**1**) ligand and its La(III) complex (**2**) are shown in Figs. 5 and 6, respectively. Examining the
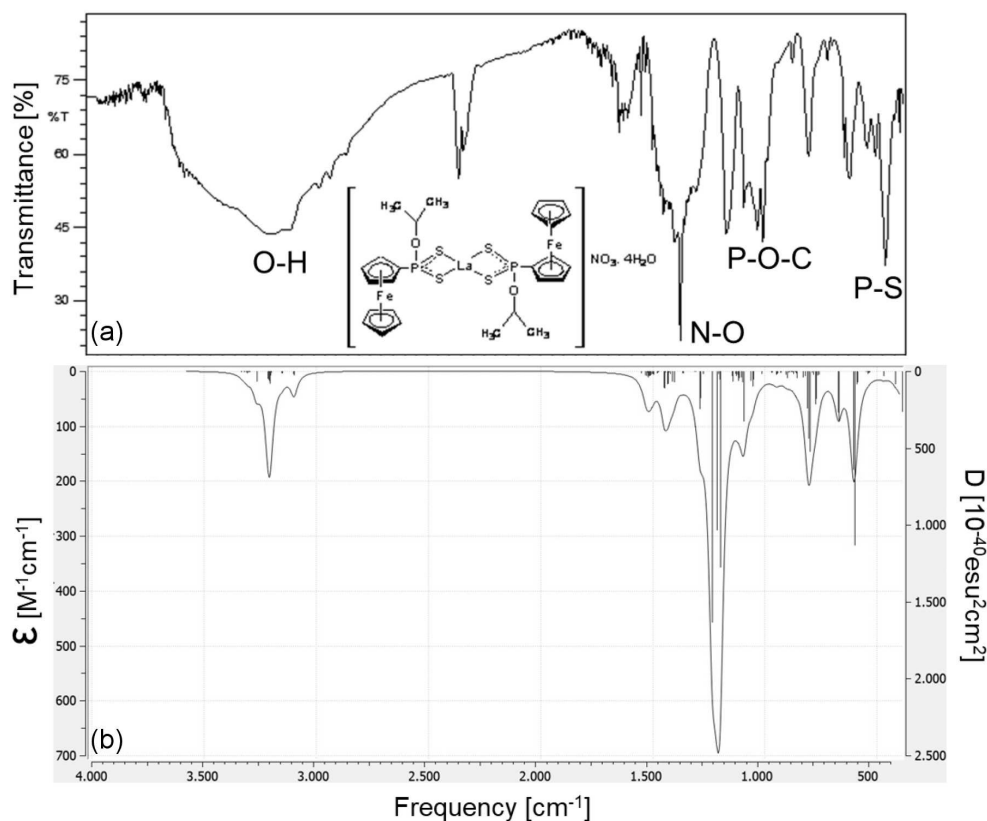
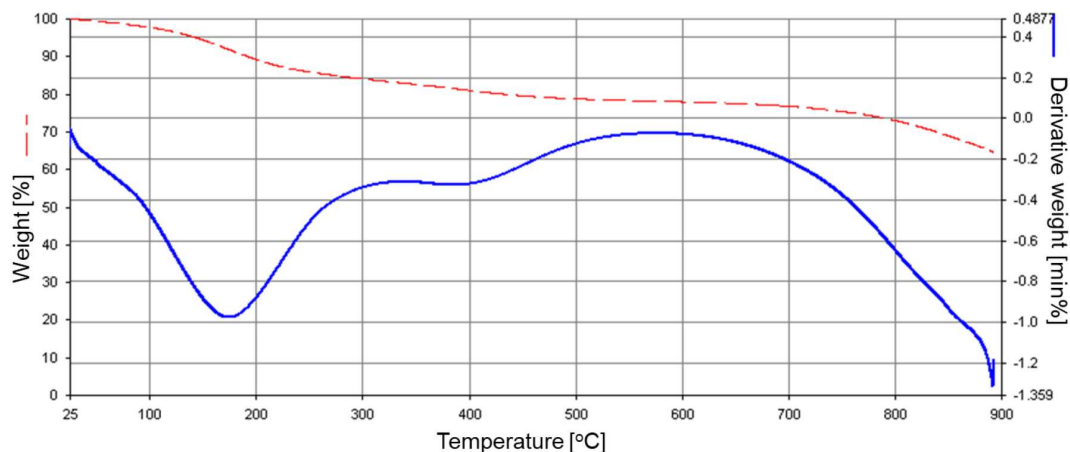Fig. 6. Experimental (a) and calculated (b) FT-IR spectra of **2**.

Fig. 7. Thermal analysis diagram of **2**.

experimental FT-IR spectrum of **1**, the stretching vibrations for the N–H and P–O–C bonds were found to be 3103 and 1105 cm^{-1}, respectively. These vibration frequencies were calculated as 3074 and 1082 cm^{-1} at the mentioned theory level, respectively. The characteristic ν_{asym}(PS) and ν_{sym}(PS) stretching vibrations of **1** were obtained at 646 (calc. 651) and 580 (calc. 552) cm^{-1}, respectively [21]. The stretching vibration of the O–H bond originating from the hydrate water molecule appeared at 3400 cm^{-1} in the FT-IR

spectrum of **2**. The N–O stretching vibration of the nitrate group in the structure was observed at 1389 cm^{-1}. Since the hydrate water molecules and nitrate group in the structure of **2** were respectively adsorbed and ionic bonded, they are not included in the optimized geometry of the complex. While the stretching vibration of the P–O–C bond appeared at 1182 cm^{-1} in the experimental spectrum of **2**, this band was calculated to be 1204 cm^{-1}. At the end of the complex formation, the characteristic ν_{asym}(PS) and ν_{sym}(PS) stretching vibrations

shifted and became 672 cm^{-1} and 563 cm^{-1}, respectively [21]. These vibrational frequencies were calculated in the theoretical spectrum at 676 and 591 cm^{-1}, respectively. From the experimental FT-IR spectrum of **2**, it was observed that the N–H stretching vibrations of **1** disappeared.

Obtained by the reaction of ferrocenyl dithiophosphonic acid ammonium salt with La(NO$_3$)$_3$ · 6H$_2$O in THF medium, the metal complex (**2**) with the general formula of [LaL$_2$]NO$_3$ · 4H$_2$O was originally synthesized. The resulting complex **2** completely dissolved in polar solvents such as DMF and DMSO, but slightly dissolved in solvents such as dichloromethane, chloroform, and benzene.

As can be seen from the thermal analysis diagram of **2** shown in Fig. 7, four moles of hydrated water were found in its structure. In the thermal analysis diagram of **2**, it was determined that there was a mass loss attributed to four moles of hydrated water at 130°C. This mass loss also confirmed the elemental analysis data and the proposed geometric structure of complex **2**.

From the ^{31}P-NMR spectra of **2**, peak diversity and flatness were observed in the chemical shift range δ = 75–20 ppm. When the ^{1}H-NMR spectrum was examined, it was observed that the details were lost, and the proton peaks of the ligand became wider [6]. The peak variation and loss of detail in the ^{1}H and ^{31}P-NMR spectra of complex **2** were due to the NMR active isotope La (^{139}La with $I = 7/2$).

However, in the phosphorus-interacted ^{1}H-NMR spectrum of complex **2** recorded in the DMSO-d$_6$ medium, it was observed that the protons in the phosphorus-linked substituted ferrocene ring and the unsubstituted ferrocene ring were within the expected chemical shift ranges in the spectrum. While the -OCH- proton in the alkyl group should be observed as peak abundance at δ = 4.41 ppm, they appeared as peak diffuseness in the spectrum. The peak at δ = 1.20 ppm was thought to belong to the methyl protons adjacent to the -CH- proton.

3.2. Computational details

The optimized geometries of **1** and **2** in the gas phase were obtained by applying the DFT/B3LYP method with a basis set of 6-311G(d, p). LanL2DZ with the effective core potential for the Fe and La atoms was used. The calculated optimized molecular geometries of **1** and **2** are shown in Figs. 8 and 9, respectively. Geometric parameters such as bond length, bond angle, and dihedral angle obtained from these geometries are given in Table II.

The bond lengths of C2-Fe11 and C7-Fe11 in the ferrocene structure in compound **1** were 2.030 Å and 2.028 Å, respectively. Although the Fe atom was not in direct coordination with the La(III) ion, these bond lengths were affected by the complex formation and extended to 2.224 Å and 2.136 Å, respectively. The C4-P12 bond shortened by 0.016 Å
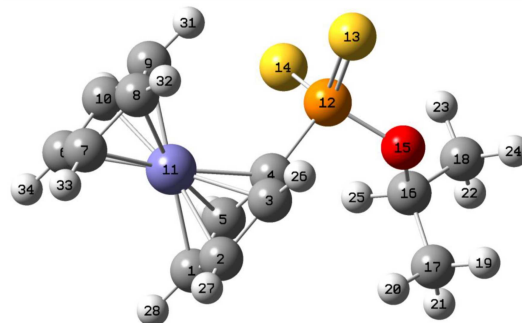

Fig. 8. Optimized molecular geometry and atomic numbering of compound **1** calculated at the DFT/B3LYP/6-311G(d,p) and DFT/B3LYP/LanL2DZ (for Fe) levels.
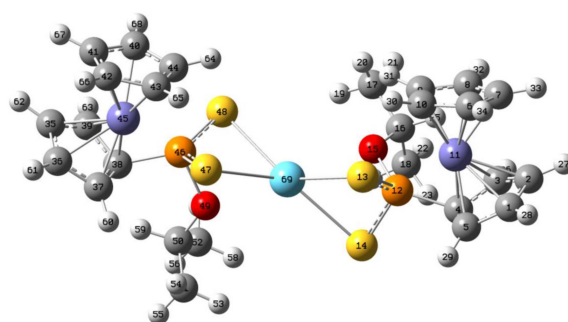

Fig. 9. Optimized molecular geometry and atomic numbering of complex **2** calculated at the DFT/B3LYP/6-311G(d,p) and DFT/B3LYP/LanL2DZ (for Fe and La) levels.

with the formation of the complex. Due to the coordination of the sulfur atoms in the ligand with La(III), the bond lengths of P12-S13 and P12-S14 lengthened by 0.088 Å and 0.073 Å, respectively. The newly formed bond lengths of S13-La69, S14-La69, S47-La69, and S48-La69 were calculated to be close to each other in the range of 2.908–2.954 Å with the formation of complex **2**.

Significant changes were also observed in some bond angles in the structure as a result of the formation of the metal complex of **1**. The C2–Fe–C7 bond angle, which was 108.3° in the ferrocene structure, decreased with the effect of possible steric hindrance and became 75.2°. The C4–P12–O15 bond angle between ferrocene, phosphorus, and oxygen in the ligand and its metal complex was calculated as 100.1° and 127.6°, respectively. After the coordination of the sulfur atoms with the La(III) ion, the S13–P12–S14 bond angle, which was 121.8° in the compound **1**, decreased to 106.9°. When the bond angles around the metal ion in the complex were examined, the bond angles of S13–La69–S14 and S13–La69–S47 were calculated to be 69.5° and 98.6°, respectively. Based on these values, it was concluded that the coordination around the metal ion was in the distorted square planar geometry.

TABLE II

Some selected calculated bond lengths [Å], bond and dihedral angles [°] for the **1** and **2** compounds at the DFT/B3LYP/6-311G(d,p) and DFT/B3LYP/LanL2DZ (for Fe and La) levels.

1		2	
Bond lengths [Å]			
C2–Fe11	2.030	C2–Fe11	2.224
C7–Fe11	2.028	C7–Fe11	2.136
C4–P12	1.834	C4–P12	1.818
P12–S13	1.985	P12–S13	2.073
P12–S14	1.998	P12–S14	2.071
P12–O15	1.673	P12–O15	1.754
C15–C16	1.432	C15–C16	1.470
C2–H27	1.084	C2–H27	1.084
C2–C3	1.425	C2–C3	1.423
C16–C17	1.524	C16–C17	1.526
C17–H21	1.098	C17–H21	1.098
		S13–La69	2.929
		S14–La69	2.908
		S48–La69	2.954
		S47–La69	2.946
Bond angles [°]			
C2–Fe11–C7	108.3	C2–Fe11–C7	75.2
C4–P12–O15	100.1	C4–P12–O15	127.6
C4–P12–S14	107.9	C4–P12–S14	105.6
C4–P12–S13	109.2	C4–P12–S13	117.0
S13–P12–S14	121.8	S13–P12–S14	106.9
P12–O15–C16	121.5	P12–O15–C16	122.6
C17–C16–C18	113.1	C17–C16–C18	112.9
		S13–La69–S14	69.5
		S14–La69–S48	139.9
		S47–La69–S48	73.7
		S13–La69–S47	98.6
Dihedral angles [°]			
C3–C4–P12–S14	−159.0	C3–C4–P12–S14	131.5
S13–P12–O15–C16	−170.8	S13–P12–O15–C16	147.8
P12–O15–C16–C17	−126.1	P12–O15–C16–C17	−162.9
		P12–S14–La69–S47	−111.3
		S13–La69–S48–O46	−109.6

The dihedral angle between the four atoms is approximately equal to 0° or 180°, meaning that these related atoms lie almost in the same plane. The dihedral angles of C3–C4–P12–S14 between ferrocene, phosphorus, and sulfur and of P12–O15–C16–C17 between phosphorus, oxygen, and isopropyl in molecule **1** were calculated to be −159.0° and −126.1°, respectively. These dihedral angle values indicated that the mentioned moieties did not lie in the same plane. Calculation of the dihedral angle of S13–P12–O15–C16 as −170.8° showed that these atoms approached the same plane. Considering the dihedral angles around the metal ion in complex **2**, the dihedral angles of P12–S14–La69–S47 and S13–La69–S48–O46 were obtained as −111.3° and −109.6°, respectively, indicating that these atoms do not lie in the same plane.
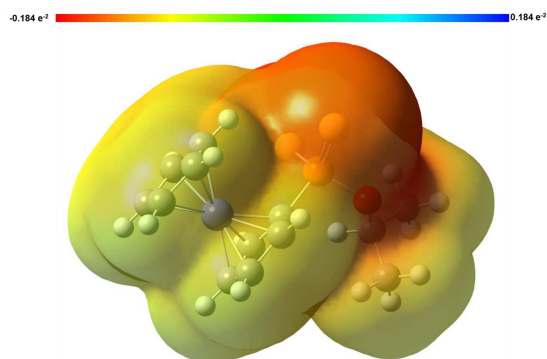

Fig. 10. MEP surface diagram of **1** calculated at the DFT/B3LYP/6-311G(d,p) and DFT/B3LYP/LanL2DZ (for Fe) levels.
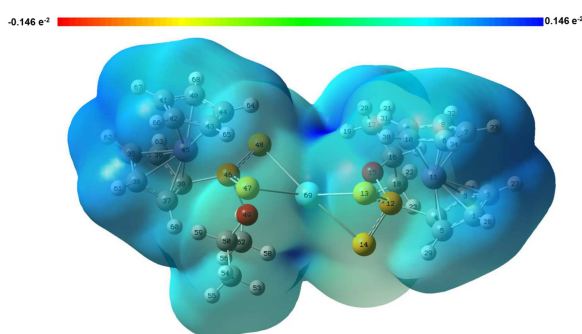

Fig. 11. MEP surface diagram of **2** calculated at the DFT/B3LYP/6-311G(d,p) and DFT/B3LYP/LanL2DZ (for Fe and La) levels.

Molecular electrostatic potential (MEP) surface diagrams of compounds are very useful for understanding their reactive sites and behavior in chemical reactions. The red regions in these diagrams are electron-rich and are responsible for the generally nucleophilic reaction of the compound. The blue regions are electron-poor and are related to the electrophilic reaction of the compound. In the MEP diagram of the optimized geometry of molecule **1**, the red zone above the sulfur atoms attracted attention (Fig. 10). This electron-rich region, caused by the electronegativity of sulfur atoms, was the nucleophilic attack site of molecule **1** in chemical reactions. The binding of the La(III) ion with the sulfur atoms of the ligand in the complex formation confirmed the result obtained from the MEP diagram of **1**. Since compound **2** is a cationic complex with a +1 charge, no significant charge density was observed in the MEP diagram of **2** (Fig. 11). Therefore, it was determined that the electric potential was homogeneously distributed throughout the molecule.

Frontier molecular orbitals are very important in terms of predicting the electrical and optical properties of compounds as well as their behavior in chemical reactions. They also help determine the
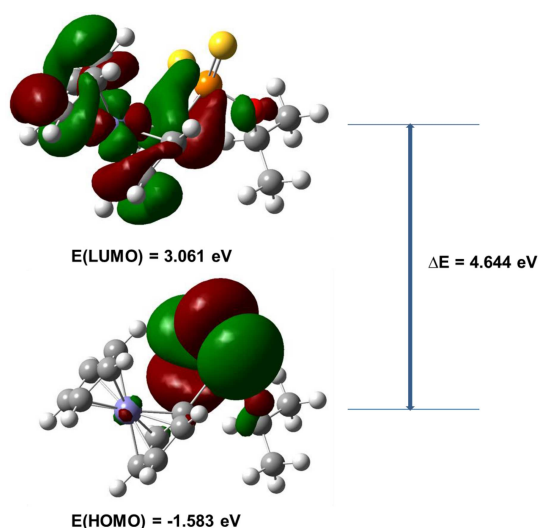
E(LUMO) = 3.061 eV

ΔE = 4.644 eV

E(HOMO) = -1.583 eV

Fig. 12. Molecular orbital surfaces and energy levels for HOMO and LUMO of compound **1** calculated at the DFT/B3LYP/6-311G(d, p) and DFT/B3LYP/LanL2DZ (for Fe) levels.

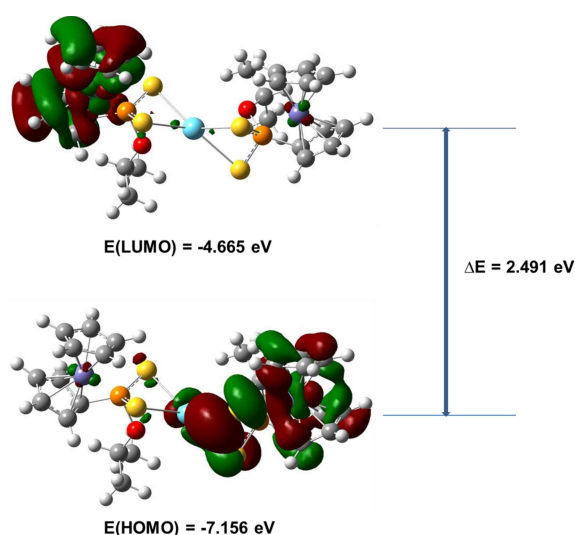

E(LUMO) = -4.665 eV

ΔE = 2.491 eV

E(HOMO) = -7.156 eV

Fig. 13. Molecular orbital surfaces and energy levels for HOMO and LUMO of complex **2** calculated at the DFT/B3LYP/6-311G(d, p) and DFT/B3LYP/LanL2DZ (for Fe and La) levels.

way the molecule interacts with other species [22]. HOMO is an orbital that mainly acts as an electron donor, while LUMO is an orbital that primarily acts as an electron acceptor. The gap between HOMO and LUMO provides important information in determining the chemical stability of the molecule [23].

The frontier molecular orbitals of **1** and **2** were calculated at the DFT level, and their HOMO–LUMO orbitals are shown in Figs. 12 and 13, respectively. The HOMOs of **1** were located throughout the molecule, mainly with the exception of the iso-propyl and ferrocene moieties. The LUMOs of molecule **1** were generally in other regions of the

molecule, except for iso-propyl and the P $=$ S group. The HOMOs of the synthesized metal complex (**2**) were mostly concentrated on La(III) ion, one ferrocene, and PS moieties, while LUMOs were located on one ferrocene and iso-propyl group. It was thought that if the **1** and **2** molecules were excited by any effect, electron transitions would take place between these HOMO–LUMO regions. On the other hand, as given in Figs. 12 and 13, the HOMO–LUMO gap energies of compounds **1** and **2** were calculated to be 4.644 and 2.491 eV, respectively. Based on these values, it was concluded that compound **2** is softer than **1** and may be more reactive in chemical reactions.

4. Conclusions

In this study, ammonium O-iso-propyl ferrocenyl dithiophosphonate and its novel La(III) complex were synthesized, and the resulting molecules were characterized using spectroscopic and thermal techniques. The results revealed that the metal:ligand ratio in the complex was 1:2. There are two sulfur atoms in the ligand — one anionic and the other neutral. It was determined that the quaternary coordination was completed as a result of the covalent bonding of the anionic sulfur in two moles of the ligand with the La(III) ion and the coordination of the other sulfur atoms with the La(III) ion. Quantum chemical calculations of both molecules were performed by the DFT/B3LYP method using LanL2DZ for Fe and La and 6-311G(d, p) basis set for other atoms. As a result of the calculations, optimized geometries, some important geometric parameters, molecular electrostatic potential surface diagrams, and HOMO–LUMOs of compounds **1** and **2** were obtained. As a result of the study, a novel La(III) ferrocenyl dithiophosphonate complex, which is relatively rare in the literature compared to other transition metals, was synthesized, and DFT calculations were performed.

References

[1] I.P. Gray, H.L. Milton, A.M. Slawin, J.D. Woollins, *Dalton Trans.* **17**, 3450 (2003).

[2] E. Mkumbuzi, W.E. van Zyl, *J. Mol. Struct.* **1226**, 129338 (2021).

[3] S. Solak, A. Ö. Kiraz, M. Karakuş, *Phosphorus Sulfur Silicon Relat. Elem.* **194**, 1054 (2019).

[4] M.R.St.J. Foreman, A.M.Z. Slawin, J.D. Woollins, *J. Chem. Soc. Dalton Trans.* **1996**, 3653 (1996).

[5] I. Haiduc, L.Y. Goh, *Coord. Chem. Rev.* **224**, 151 (2002).

[6] E.G. Sağlam, Ö. Çelik, H. Yılmaz, S. Ide, *Trans. Metal Chem.* **35**, 399 (2010).

[7] Y. Fan, F. Zhang, *Adv. Opt. Mater.* **7**, 1801417 (2019).

[8] J.C.G. Bünzli, *Chem. Rev.* **110**, 2729 (2010).

[9] N.S. Chundawat, S. Jadoun, P. Zarrintaj, N.P.S. Chauhan, *Polyhedron* **207**, 115387 (2021).

[10] W.N. Wu, W.B. Yuan, N. Tang, R.D. Yang, L. Yan, Z.H. Xu, *Spectrochim. Acta A Mol. Biomol. Spectr.* **65**, 912 (2006).

[11] A. Aydin, S. Özarslan, *J. Mol. Struct.* **1222**, 128861 (2020).

[12] W.E. van Zyl, J.P. Fackler, *Phosphorus Sulfur Silicon Relat. Elem.* **167**, 117 (2000).

[13] W.E. van Zyl, J.D. Woollins, *Coord. Chem. Rev.* **257**, 718 (2013).

[14] A. Aydin, N. Acar, H. Yilmaz, *Suleyman Demirel Univ. J. Sci.* **3**, 205 (2008).

[15] M.J. Frisch, G.W. Trucks, H.B. Schlegel et al., Gaussian 09 (now Gaussian 16), Gaussian Inc., Wallingford (CT) 2016.

[16] R. Dennington, T.A. Keith, J.M. Millam, GaussView, Revision 5.0.9, Semichem Inc., Shawnee Mission (KS) 2009.

[17] A.D. Becke, *J. Chem. Phys.* **98**, 5648 (1993).

[18] C. Lee, W. Yang, R.G. Parr, *Phys. Rev. B* **37**, 785 (1988).

[19] P.J. Hay, W.R. Wadt, *J. Chem. Phys.* **82**, 270 (1985).

[20] J.P. Merrick, D. Moran, L. Radom, *J. Phys. Chem. A* **111**, 11683 (2007).

[21] P. Çekirdek, A.O. Solak, M. Karakuş, A. Aydın, H. Yılmaz, *Electroanalysis* **18**, 2314 (2006).

[22] I. Fleming, *Molecular orbitals and organic chemical reactions*, John Wiley & Sons, 2011.

[23] K. Fukui, *Science.* **218**, 747 (1982).